KSCE Journal of Civil Engineering (2020) 24(8):2435-2448
DOI 10.1007/s12205-020-0255-3

pISSN 1226-7988, eISSN 1976-3808
www.springer.com/12205

Structural Engineering

Evaluation of Fracture Process Zone in the Flexural Response of Different Concrete Materials Using DIC Method

Shengtao Li[a], **Xudong Chen**[a], **and Shengshan Guo**[b]

[a]*College of Civil and Transportation Engineering, Hohai University, Nanjing 210098, China*
[b]*China Institute of Water Resources and Hydropower Research, Beijing 100048, China*

ARTICLE HISTORY

Received 12 February 2019
Revised 1st 4 October 2019
Revised 2nd 6 December 2019
Accepted 19 April 2020
Published Online 30 June 2020

KEYWORDS

Digital image correlation
Fracture process zone
Crack propagation
Rubber concrete
Pervious concrete
Self-compacting rubber concrete

ABSTRACT

In the present paper, a digital image correlation (DIC) method is used to study the development of fracture process zones (FPZ) of different concrete materials in three-point bending test. Different concrete materials including original concrete, rubber concrete, self-compacting rubber concrete and pervious concrete are investigated. Firstly, the image of the FPZ and the crack opening displacement (COD) in FPZ is obtained by acquiring strain field and displacement field information. The relationship between the development of FPZ and the mechanical properties is further studied. It is found that there is a strong correlation between the FPZ and the post-peak strength reduction of concrete. The development characteristics of FPZ of different concrete materials are analyzed. The addition of rubber will result in stronger strain concentration in pre-peak stage compared to original concrete, and the FPZ will emerges at the earlier loading stage, but it can enhance the crack resistance of concrete in the post-peak stage. Self-compacting rubber concrete was observed to have higher bearing capacity and cracking resistance during fracture than that of the others. Pervious concrete has weak resistance to fracture, and there is almost no decline of the FPZ development rate in fracture process.

1. Introduction

The application of the concrete is widespread in construction of infrastructure thanks to its low production cost, good formability and heat-resistant (Guan et al., 2019). However, the brittle nature of concrete and its low tensile strength compared to other materials make concrete vulnerable to fracture in tension. The crack resistance is a fundamental property to investigate the fracture behavior of concrete (Xu and Zhang, 2008). As is well-known, quasi-brittle materials such as concrete and rock have a different fracture characteristic from brittle fracture (Galouei and Fakhimi, 2015). In brittle fracture, the energy applied on the material is mainly consumed on the formation of a new crack surface, which is much larger than the energy of forming the plastic zone inside the material. The linear elastic fracture mechanics can be used to analyze this fracture process and crack development (Ghamgosar and Erarslan, 2016). However, a large part of the energy applied to the concrete is used to form the fracture process zone (FPZ) (Carpinteri et al., 2017). The FPZ is the concentrated area of microcracks adjacent to the crack tip. When subjected to tensile stresses larger than the tensile strength of the concrete, the microcracks will appear before the stress-strain curve reaches the peak and become macroscopic cracks as the softening process proceeds until the fracture occurs. Therefore, the evolution of FPZ is usually divided into two main stages, the pre-critical crack growth and the unstable crack propagation (Dong et al., 2013). A true identification of FPZ (its length, width and shape) is important for understanding the mechanism of concrete degradation and the loss of bearing capacity. In fracture mechanics theory, fracture occurs when the stress intensity (usually called K_I) exceeds the limit state, i.e., the critical value (K_{IC}), which is called fracture toughness (Kim and El Hussein., 1997). Fracture energy (G_F) is defined as the area under the post-peak stress versus crack opening displacement curve (Jenq and Shah, 1985). These two important fracture parameters (K_{IC} and G_F) are also directly related to the mechanical properties of the FPZ (Hu and Wittmann, 1992). In the numerical calculation of concrete fracture, it is important to

CORRESPONDENCE Xudong Chen cxdong1985@hotmail.com College of Civil and Transportation Engineering, Hohai University, Nanjing 210098, China

select appropriate expansion criteria and apply correct cohesive stress on the FPZ. However, the parameters of the size and softening curve of the FPZ are difficult to obtain from the experiment. Therefore, it is particularly important to carry out research on the mechanical properties of the FPZ and the expansion criteria (Zhang and Ansari, 2005).

There are many factors affecting the mechanical properties of the fracture process, including the depth and the width of concrete specimen, loading rate, initial crack length and aggregate size (Saouma et al., 1991; Meng et al., 2017). Wu et al. (2011) found that the length of the FPZ increases with the height of the concrete and decreases with the notch length. Dong et al. (2018) found that the length of the FPZ is affected after the creep of concrete. The effects of maximum aggregate size and the size of the specimen on the length and width of FPZ were investigated (Otsuka and Date, 2000). However, these studies were conducted to investigate the development of FPZs of plain or original concrete (OC). With the development of concrete materials, new concrete materials have been received more attention and application (Marar et al., 2017; Sayadi et al., 2018). It has been noted that rubber concrete (RC) can absorb more energy and improve the impact and fatigue resistance of structures (Thomas and Gupta, 2015; Xu et al., 2018). Accordingly, rubber concrete and self-compacting concrete were combined to form self-compacting rubberized concrete (SCRC) to enhance the workability and the strength of rubber concrete with a rubber content of 5% – 30% of the fine aggregate as well as the addition of the fly ash and superplasticizer (Bignozzi and Sandrolini, 2006; Yung et al., 2013). Pervious concrete (PC) achieves good permeability by removing fine aggregates (Ibrahim et al., 2014; Yuan et al., 2018). These materials are gradually used in engineering construction for they can relieve environmental pressure in cities (Yang and Jiang, 2003; Reda Taha et al., 2008). However, few people have studied the fracture behavior and development characteristics of fracture process zones in these concrete materials. The study of FPZ for different concrete materials can provide more comprehensive information for understanding the nature of the FPZ.

Digital image correlation is an optical technique used to obtain the information of the surface deformation field of the measured object (Rechenmacher and Finno, 2004). The displacement of each speckle in the image is obtained by comparing the images before and after deformation (Marar et al., 2017; Sayadi et al., 2018). This method has the characteristics of wide measurement range and high accuracy (Kozicki and Tejchman, 2007). It can be used as a powerful tool in the monitoring of structures. However, some factors, such as lighting fluctuations, speckle pattern, out-of-plane movement, subset size, algorithm, locations of control points, etc., may affect the accuracy of this technology, and many studies have proposed solutions to these problems (Yaofeng and Pang, 2007; Yang, 2014; Zhu et al., 2015). So far, DIC has been used in the surveys of crack development (Gali and Subramaniam, 2017), bridge displacement (Kim et al., 2013), the crack width measurement (Mirzazadeh et al., 2016) and the deflection measurement of the beams (Mirzazadeh and Green, 2018). The results of these studies prove that DIC can be well applied to observe the FPZ of concrete.

In this paper, DIC method was used to study the development of FPZ of four different concrete materials. Three-point bending experiments were conducted. The morphology of the FPZ and the crack opening displacement at different loading stages were obtained by the surface strain field and the displacement field. Based on the above experimental results, the characteristics of the development of FPZ and the corresponding mechanical response were obtained. The differences of FPZs of different materials were discussed. The experiments in the present paper will help to better understand the influencing factors and mechanisms of the fracture characteristics of concrete. In addition, the characteristics of the FPZ and crack opening displacement provided in this paper will contribute to the theoretical analyses and numerical analyses of the fracture process of these concrete materials.

2. Materials and Methods

2.1 Experimental Material and Mix Proportion

Four different concrete materials were used in this paper, namely original concrete (OC), rubber concrete (RC), self-compacting

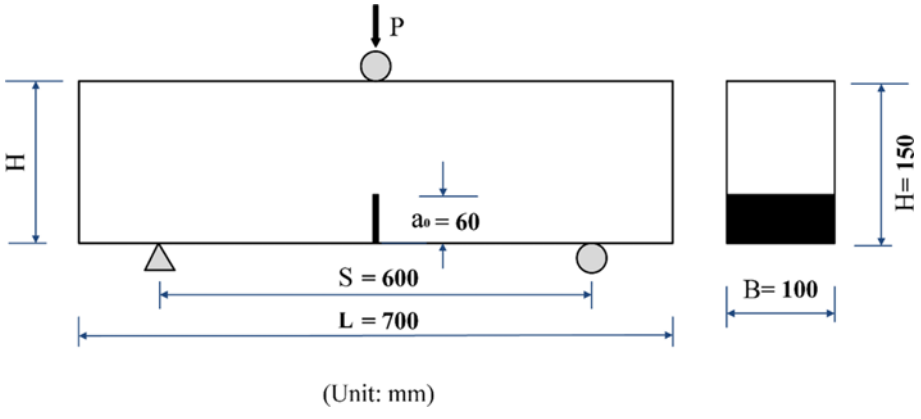

Fig. 1. Loading Mode of Specimen

Table 1. Mix Proportions of Concretes (kg/m^3)

Materials	Original concrete (OC)	Rubber concrete (RC)	Self-compacting rubberized concrete (SCRC)	Pervious concrete (PC)
Portland cement	358	358	385	420
Gravel	1,210	736	800	1,550
Sand	919.4	919.4	916.2	-
Water	177	177	200	126
Fly ash	90	90	139	-
Rubber	-	7.5	41.5	-
Silica fume	-	-	26	-
Water-reducer	4.31	4.31	7.30	2.52

rubber concrete (SCRC) and pervious concrete (PC). The dimension of the specimens was 700 × 150 × 100 mm, and it is shown in Fig. 1, where the length (L) of the beam is 700 mm, the span (S) 600 mm, the height (H) 150 mm, and the thickness (B) 100 mm. There was a notch of which the width was 2 mm in the mid-span of the specimen, and a_0 was the length of the notch which equal to 60 mm.

The ingredients of the specimens used in the tests are shown in Table 1. The rubber particle size used in the experiment was 0.5 mm, and the density was 1,060 kg/m^3. The rubber particle content accounted for 2% of the total sand volume in rubber concrete. The content of rubber particles in self-compacting rubber concrete accounted for 10% of the total sand volume.

2.2 Digital Image Correlation Technique

DIC is an effective measuring method to visualize deformations of the photographed surface. It can obtain the displacements of the points in digital images. DIC divides each area of interest in the image into small overlapping sub-areas called search patches (Kozicki and Tejchman, 2007). In order to calculate the displacement, it is necessary to determine the correlation between the image subsets from undeformed stage to deformed stage. The undeformed point (x, y) is mapped to the deformed point (x_1, y_1). By minimizing the correlation coefficient C, the horizontal displacement u and the vertical displacement v of the surface analysis region are obtained (Zhao et al., 2017).

In this study, the surfaces of the specimens were sprayed with paint to produce random black and white speckles. These randomly arranged speckle are helpful for image correlation processing. Two CCD cameras were chosen to conduct the tests with a resolution of 2,048 × 2,048 pixel. The camera lenses were nearly perpendicular to the surface of the specimen and were 1.5 m away from the surface (as shown in Fig. 2). The loading process and the photo acquisition began at the same time until the failure of the specimen. During the experiment, the cameras collected two pictures per second and saved them in TIF format automatically. According to the time interval, the time point at which the digital image was taken during the experiment can be calculated. The image and the P-CMOD curve can be corresponded accordingly.

After the experiment, the appropriate image processing area in which the crack is expected to grow is selected in the VIC-3D software (as shown in Fig. 2), and the displacement field of the specimen surface is obtained by the calculation of the software. Considering the accuracy and efficiency of calculation, the size

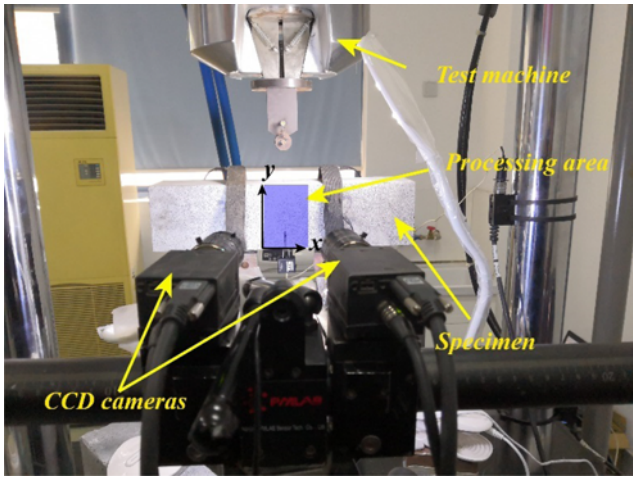

Fig. 2. Scheme of Setup

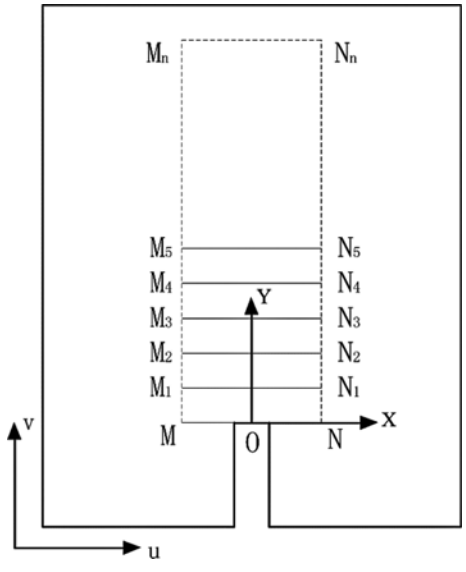

Fig. 3. The Calculation Area of Specimens Using DIC Method in the VIC-3D Software

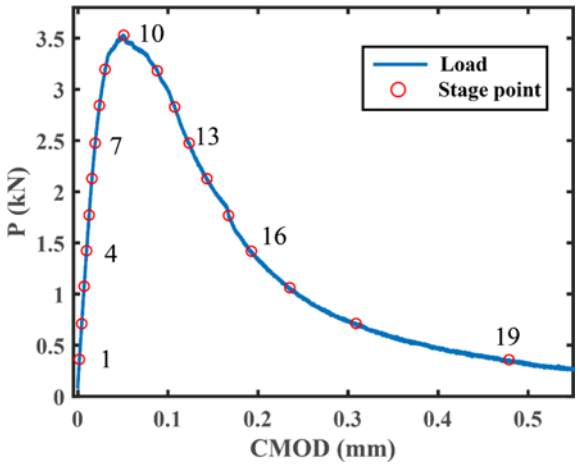

Fig. 4. Scheme of the Loading Process and Selection of DIC Observation Points

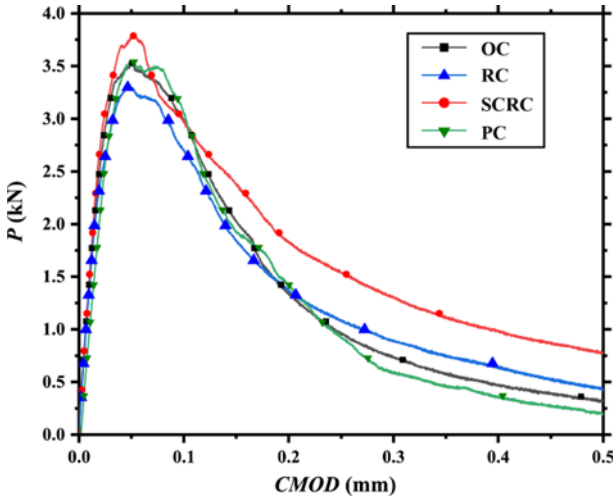

Fig. 5. Load-Displacement Curves of Different Concrete Materials

of the subset is 20 pixels and the step size is 7 pixels. In Fig. 3, the calculation area is described in detail which is represented by a blue area in Fig. 2, where X direction is the direction along the length of the beam and Y direction is the direction along the height of the beam. In the calculating area, straight lines are set as measuring lines at equal distance in the whole fracture ligament from the crack tip to the specimen tip. The displacement information will be extracted from these lines. The MN line is tangent to the notch tip, and Lines M_1N_1, M_2N_2…M_nN_n were all parallel to line MN. The distance between the adjacent lines is 7 pixels.

During the loading process, the deformation of the specimen changed with the loading, and the FPZ also developed continuously. In order to observe the appearance and propagation of the FPZ, the pre-peak and post-peak processes of the specimen were divided into several segments. Considering the simplicity of processing and the accuracy of observation, the value of the 10% peak load was chosen as the interval of the points (as shown in Fig. 4). By analyzing and comparing the deformations at each loading point, the development process of FPZ was obtained.

3. Results

The tests were conducted under three-point bending loading. The loading was controlled by the crack mouth opening displacement (CMOD). The specimen was monotonically loaded to failure at a fixed CMOD-growth rate (0.005 mm/s), and the peak load P_{max} were obtained. The load-CMOD responses of specimens of different concrete materials are shown in the Fig. 5. The experimental results showed that the flexural bearing capacity of the rubber concrete specimen was lower than that of the original concrete. The bearing capacity of pervious concrete beam was close to that of the original concrete, and the peak load value of the self-compacting rubberized concrete was the highest. When concrete only blend with rubber, it can reduce the flexural bearing capacity of the specimen. The mechanical effect of rubber blending is mainly in the post-peak section where cracks develop, and it can be observed that the tail of the load vs CMOD curve is more gentle compared to the other concrete materials. This phenomenon is more obvious in self-compacting rubberized concrete with larger rubber content.

In this paper, the fracture parameters (K_{IS}^{S} and G_F) of various concrete materials were calculated and compared. First the linear elastic compliance C_i (called initial compliance) was calculated (as shown in Table 2). To acquire the initial compliance, the data of load against CMOD was first extracted in a range of CMOD from 0.00 to 0.01 mm in order to fit the experimental data with a line (Carpinteri et al., 2017). The initial compliance value was computed by using the least squares method. The Young's modulus was obtained in the Eq. (1) (Jenq and Shah, 1985).

$$E = \frac{6Sa_0V(\alpha_0)}{C_iH^2B} \tag{1}$$

where the parameters $V(\alpha_0)$ and α_0 given by (Shah, 1990):

$$V(\alpha_0) = 0.76 - 2.28\alpha_0 + 3.87\alpha_0^2 - 2.04\alpha_0^3 + \frac{0.66}{(1-\alpha_0)^2} \tag{2}$$

Table 2. Elastic Modulus E, Compliance C_i & C_u, Peak Load P_{max}, Critical Crack Length a_c, Critical Stress-Intensity Factor K_{IC}^{S}, Fracture Energy G_F

Types of concrete	C_i (mm/N)	E (GPa)	P_{max} (KN)	C_u (mm/N)	a_c (mm)	K_{IC}^{S} (MPa·m$^{1/2}$)	G_F (N/m)
OC	7.4	28.87	3.53	14.3	78.4	1.096	97.6
RC	7.2	29.77	3.30	14.0	66.9	0.922	99.25
SCRC	6.6	32.15	3.79	16.6	84.9	1.185	133.4
PC	8.2	25.96	3.54	16.4	79.1	1.023	77.5

and α_0 is the coefficient related to a_0, where $\alpha_0 = (a_0 + h_0)/(H + h_0)$, a_0 is the initial notch depth, and h_0 is the thickness of holder of clip gauge, which is 2 mm in this study. The critical effective crack length a_c is defined as the effective crack length at the peak load in concrete fracture mechanics, which can be calculated after obtaining the E value from the following equation (Shah, 1990):

$$E = \frac{6Sa_cV(\alpha)}{C_uH^2B} \tag{3}$$

the corresponding flexibility value of 95% residual load after peak was selected from the P-CMOD curve as the C_u value, in $V(\alpha)$ (Shah, 1990):

$$\alpha = (a + h_0)/(d + h_0) \tag{4}$$

the critical stress-intensity factor is computed by using the following equation:

$$K_{IC}^{S} = 3(P_{max} + 0.5W)\frac{S(\pi a_c)^{1/2}F(\alpha)}{2H^2B} \tag{5}$$

in which,

$$F(\alpha) = \frac{1.99 - \alpha \times (1-\alpha) \times (2.15 - 3.93 \times \alpha + 2.7\alpha^2)}{\pi^{0.5} \times (1+2\alpha) \times (1-\alpha)^{1.5}} \tag{6}$$

where $\alpha = a_c/H$, P_{max} = the peak load [N], $W = W_0S/L$, W_0 is equal to self-weight of the beam [N].

Fracture energy (G_F) is calculated by the suggestion of RILEM (Wittman, 1985) given in Eq. (7):

$$G_F = \frac{W_1 + W_0\delta}{A} \tag{7}$$

where W_1 is the area under the load-CMOD curve (N/m), δ is the maximum displacement (m), and A is the fracture area which is $(H - a_0)B$ (m^2) (Arslan, 2016). The Young's elastic modulus and fracture parameters of the materials are shown in the Table 2. The Young's elastic modulus of self-compacting rubber concrete is the largest, and the modulus of rubber concrete is larger than that of plain concrete, while that of pervious concrete is the smallest. The fracture parameters calculated by the above method show that the critical stress-intensity factor of the RC is lower than OC. This indicate that the fracture toughness of concrete may decrease with only rubber as the addition. However, the value of SCRC is higher than that of OC, which shows that presence of silica fume and fly ash in SCRC may contribute to the critical stress-intensity factor increase. The results of PC shows that the removal of mortar may also reduce the fracture toughness. It is also observed that the addition of rubber can increase the fracture energy. In the self-compacting rubber concrete, the increase of fracture energy was higher than rubber concrete because higher amount of rubber particles is added. The corresponding fracture behaviors of these concrete materials were observed, and the mechanism will be described in detail later.

3.1 Determination of the FPZ

In the three-point bending test, the crack usually appeared vertically in Mode I fracture due to the tensile stress. There is a microcracking region ahead of the notch tip at first, where microcracks extend and finally form macrocracks. It is the FPZ which develops around the notch tip and generate dramatic displacement change in the material. The discontinuous deformation causes the strain value calculated by DIC to be relatively high, ranging from hundreds to thousands micro strain. Fig. 6(a) shows a typical 3D plot of strain field of a specimen at the peak load stage. It can be seen that a distinct peak appears ahead of the notch tip in the figure, indicating that that strain concentration occurs there. The Fig. 6(b) shows the 2D image of the strain concentration area around the notch tip corresponding to Fig. 6(a). It can be observed that there are also some strain concentration appearing in other regions, which are caused by the heterogeneity of the materials. However, it can be seen from Fig. 6(a) that the strain values in these areas are much smaller than those at the notch tip, which is more obvious in the subsequent development of FPZ. This indicates that the information of these areas as shown in Fig. 6(a) is far less important than that in FPZ. We

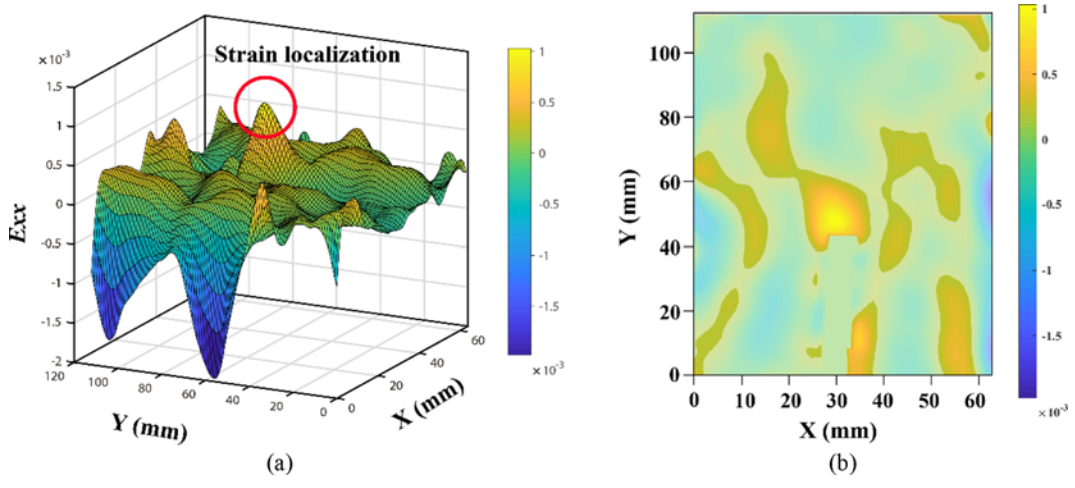

Fig. 6. Surface Strain Field of Original Concrete at Peak Load Stage: (a) 3D Plot, (b) 2D Contour

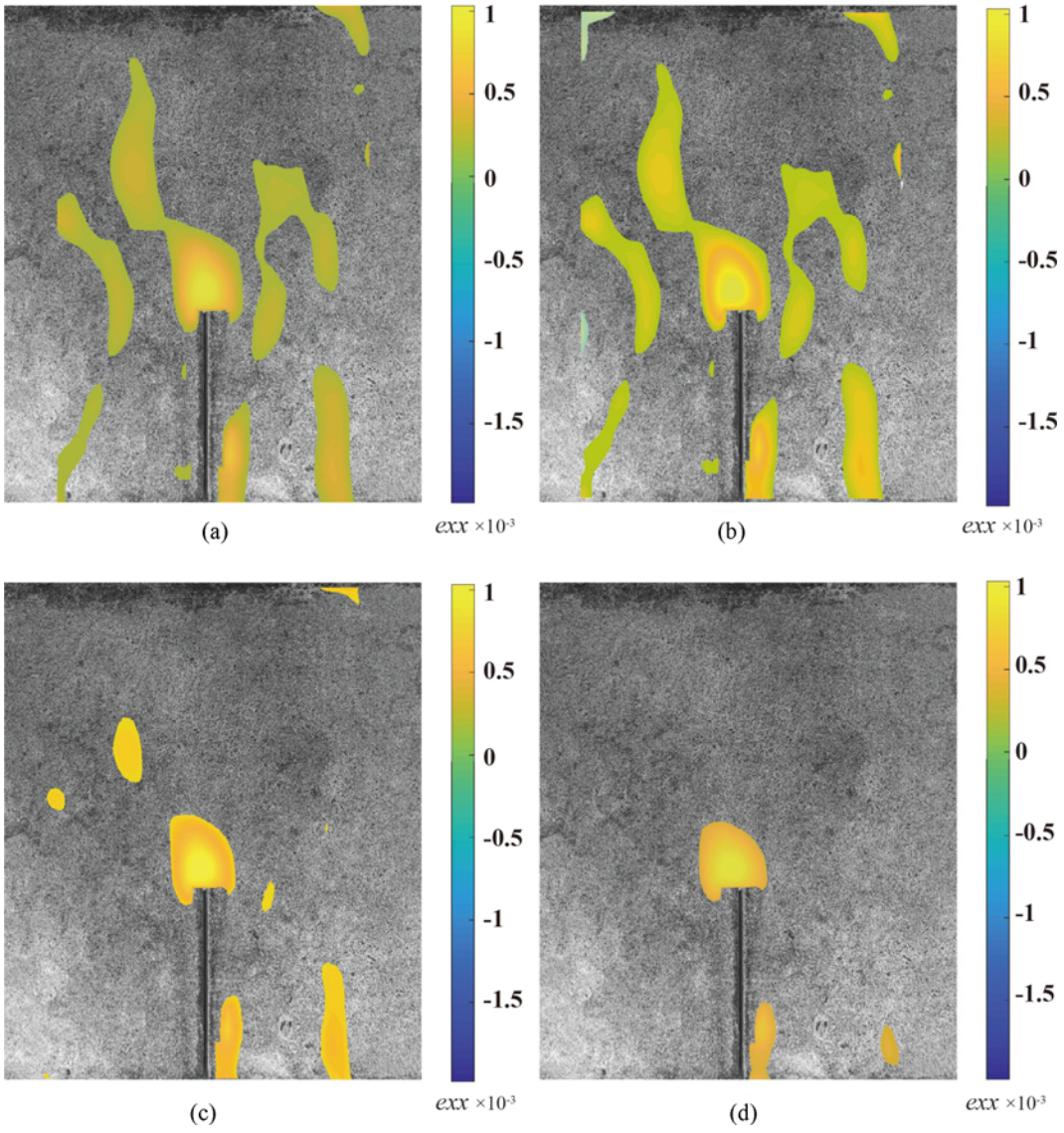

Fig. 7. Comparison of Surface Strain Field of Plain Concrete Specimen under Different Strain Thresholds at Peak Load Stage: (a) 100 εμ, (b) 200 εμ, (c) 300 εμ, (d) 400 εμ

therefore consider filtering out the interference in these other areas to better study the fracture process area. In this paper, the strains were calculated with DIC first, then an appropriate threshold was found and set to estimate the strain concentration area. The size and shape of the FPZ are determined by visualization of the data. The effective crack length is regarded as length of the existing notch plus length of the FPZ. Based on this, the variation of the effective crack length on the surface of the different concrete specimens was compared to evaluate the fracture characteristics. Under different strain thresholds, the size of the FPZ is different. The appropriate threshold should be able to obtain the expected FPZ and it is essential for the later analysis of fracture performance. The Fig. 7 shows the strain contour with different thresholds of a concrete specimen at the peak load. For the 100 – 200 microstrain, in addition to the notch tip region, other regions on the surface of the specimens also had many colored areas, indicating the strains in these regions is relatively high. The strain value in these areas was between 200 – 300 microstrain. And during the experiment, the values of the microstrain in these areas were always fluctuating around 200 – 300 microstrain, indicating that the observed strain was not the true strain caused by the load. Previous studies have found that there are small errors in strain contour measured by DIC in some areas, usually due to different DIC parameter settings such as interpolation methods, sub-region size and step size (Rossi et al., 2015). This leads to virtual strain in local regions. In order to remove the interference of these noises on the observation of the FPZ, the threshold setting should be larger than 200 microstrain. Finally, 300 microstrain is selected as the threshold segmentation criterion, so that the disturbance of small error on the graphical boundary of the FPZ can be controlled within acceptable limits.

3.2 Calculation of Crack Opening Displacement Value

During loading process, micro-cracks develop in FPZ above the notch. These micro-cracks gradually expand and join to form macroscopic cracks. The surface information of the specimens obtained by DIC is used to observe displacement and strain fields in FPZ. In this paper, the crack displacement along the height of the specimen is calculated by the surface displacement field of the specimen measured by the DIC method. Figs. 8(a) and 8(b) are respectively 3D and a 2D views of the displacement field of the original concrete beam at the loading stage 19, i.e., the last selected point in Fig. 4 with a load of 0.35 kN. The X direction is the length direction of the specimen, and the Y direction the height direction of the specimen. The U_x represents the horizontal displacement value of each point on the surface of

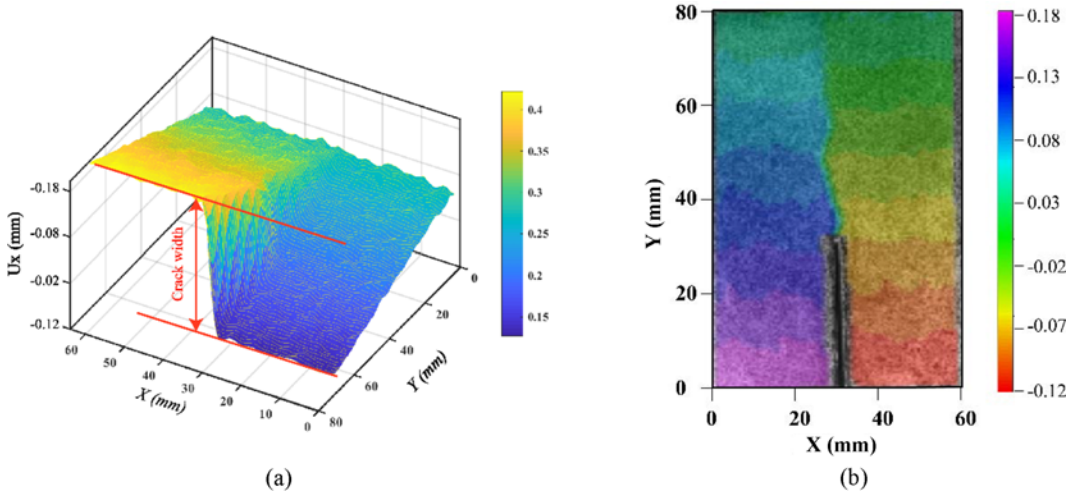

Fig. 8. Surface Displacement Field of Original Concrete: (a) 3D Plot, (b) 2D Contour

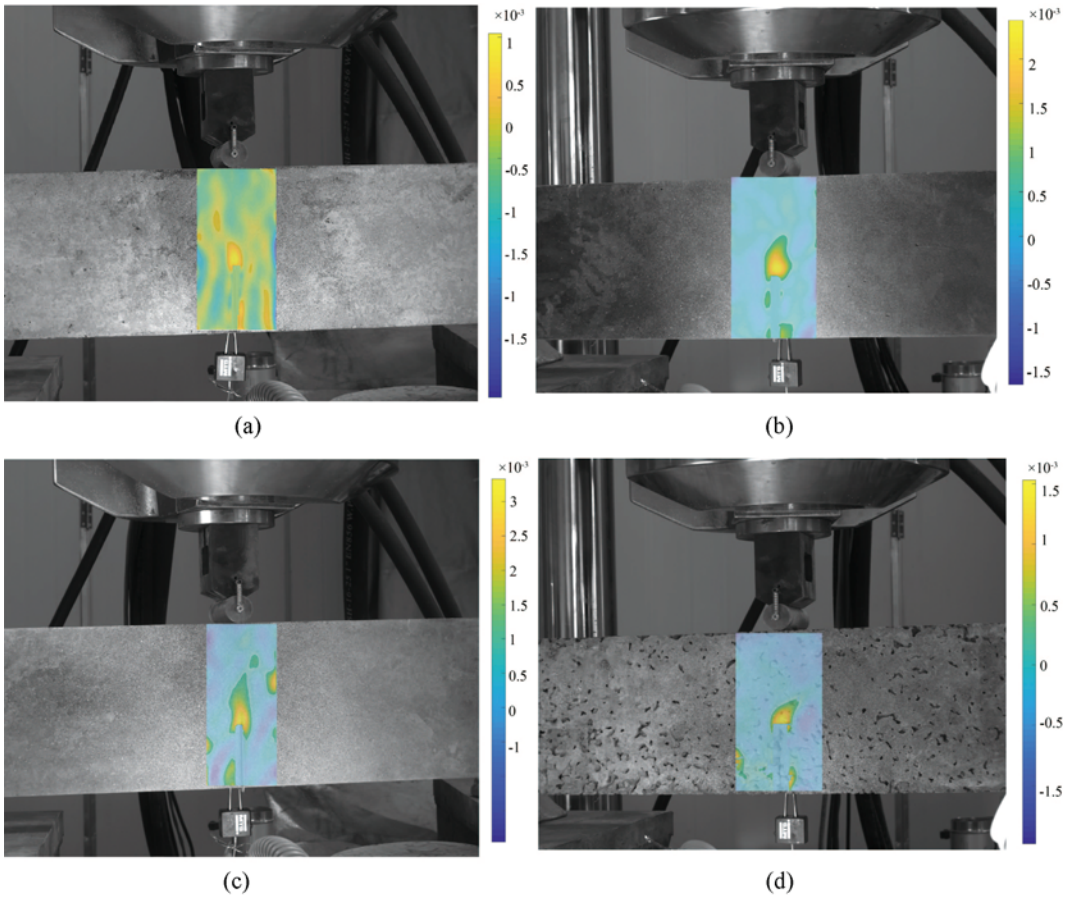

Fig. 9. FPZ Morphology of Different Concrete Materials at Peak Load: (a) Plain Concrete (P_{max} = 3.53 kN), (b) Rubber Concrete (P_{max} = 3.30 kN), (c) Self-Compacting Rubber Concrete (P_{max} = 3.79 kN), (d) Pervious Concrete (P_{max} = 3.54 kN)

the specimen. As shown in the Fig. 8(a), there is a sudden change of displacement in the mid-span, corresponding to the color change in the Fig. 8(b). This change is due to the crack opening. To calculate the crack opening, the images of the beams before and after deformation taken during a test were used. First, two columns of subsets are placed on either sides of the crack on an image taken of the cracked beam, then the same two columns of subset were placed on the undeformed image of the same beam. The distances of the two adjacent subsets located on either side of the crack before and after development of the crack were calculated and then subtracted to find the COD. This method has been used to measure deformations in reinforced concrete beams, and more detailed information about this method can be found in the works by Mirzazadeh and Green (2018). Theoretically, the horizontal displacement in the mid-span of the beam should be zero. However, with the load increasing, the roller at the experimental support will slightly shift left or right, which makes the specimen have a rigid body displacement to the left or right in the experiment. The data was corrected by subtracting the displacement from the rigid body displacement in present study (i.e., the horizontal displacement in the mid-span of the specimen). It should be noted that the data processing does not affect the COD results, because the crack width is calculated as the relative displacement between two sides of the crack as mentioned, and the rigid body displacement will be eliminated in the calculation.

3.3 The Fracture Process Zones at Peak Load Stage

Figure 9 shows the strain field of FPZ around the notch tip of each concrete material at peak load stage. As can be seen from Fig. 9, when the load reaches the ultimate load, the area of strain concentration of different specimens is various in size. Original concrete has a small FPZ with a width of 15.8 mm. The FPZ width of pervious concrete and rubber concrete is close to each other, which is 17.5 mm and 17.6 mm, respectively. The FPZ of self-compacting rubberized concrete is the widest, which is 18.9 mm. The degree of damage of the interface at the peak load stage of each specimen is determined. The initial ligament length is defined as the depth of the beam minus the depth of the initial notch, which is equal to 90 mm in present study. The ratio of the FPZ length to the initial ligament length at peak load stage is named R1. It is taken as a parameter to reflect the damage state of the cross section. The R1 value of different concrete materials are shown in Table 3. It can be seen that the R1 ratio of rubber concrete is the largest, followed by self-compacting rubberized concrete, and the value of original concrete and pervious concrete is close. It can be found that the incorporation of rubber will increase the development degree of FPZ at the peak load stage, which will be discussed in detail later.

Table 3. FPZ Length and width at Peak Load of Different Concrete Materials (mm)

Specimen	FPZ length	R1 (%)	FPZ width
OC	20.2	22.4	15.8
RC	41.6	46.2	17.5
SCRC	35.3	39.2	18.9
PC	20.1	22.4	17.6

Note: R1 = FPZ length at peak load/initial ligament length

3.4 The Crack Opening Displacement at Different Loads

With the development of FPZ, micro-cracks will appear at the notch tip, and widths of micro-cracks will increase continuously during loading process. The widths of micro-cracks can also reflect the damage state of the cross-section, because they are one of the indicators of the fracture characteristic of a concrete structure (Guo et al., 2019). In this paper, the crack width of positions above the notch is called crack opening displacement (COD) as shown in Fig. 10. Distribution of COD along the crack

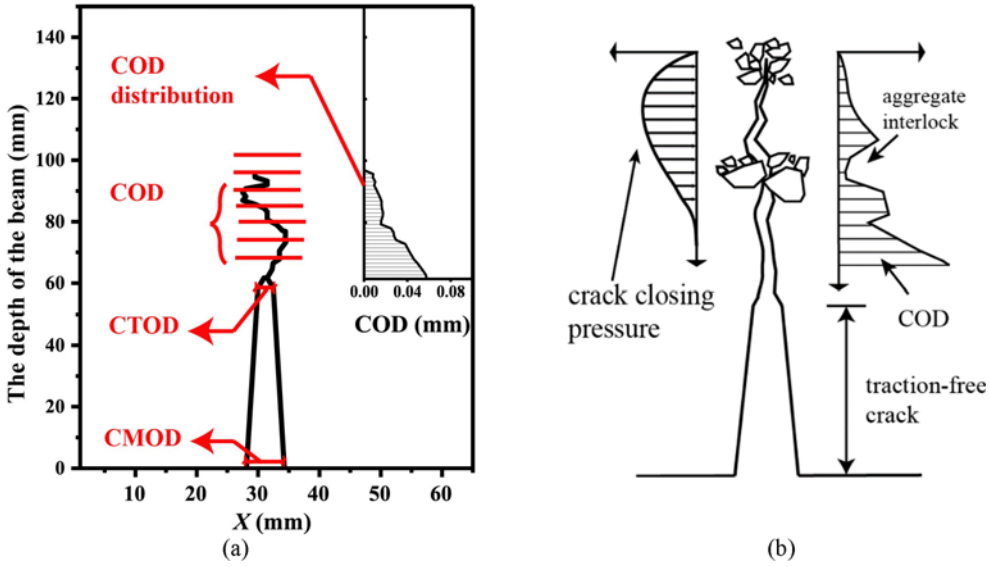

Fig. 10. Schematic Diagram of Crack Width: (a) Parameters of Crack Opening Displacement, (b) The Schematic Diagram of COD Distribution

Table 4. The COD Distribution along Depth of Beams of Different Concrete Materials at Peak Load

Materials	Load (kN)	CMOD (μm)	CTOD (μm)
Original concrete	3.53	50.8	18.5
Rubber concrete	3.3	46.4	21.0
Self-compacting rubber concrete	3.79	52.0	29.1
Pervious concrete	3.54	52.3	16.2

length can be obtained by extracting displacement data from MN lines as shown in Fig. 2, and this method is used in the present study (Wu et al., 2011). In the vicinity of the notch tip, crack opening displacements are relatively large. It can be observed that the further from the tip of the initial notch, the lower the COD (as shown in Fig. 10(a)). With the crack deflection, micro-cracking and aggregate bridging in FPZ, the slope of the COD curve may change or fluctuate sharply along the direction of the crack length, and this reflects the resistance of materials to cracks (as shown in Fig. 10(b)). The values of CMOD (the displacement of the notch mouth) and CTOD (the displacement of the notch tip) of beams with different concrete materials at the maximum load are given in Table 4. It can be seen that the CMOD values of specimens with different materials are close, which are all around 51 μm. The CMOD of rubber concrete is smaller than that of original concrete, while both pervious concrete and self-compacting rubber concrete have higher values than original concrete. The bearing capacity and CMOD of rubber concrete are both lower than those of ordinary concrete, but its CTOD is 13.5% higher than that of ordinary concrete. For self-compacting rubber concrete, the CTOD value is 56.8% higher than that of ordinary concrete. These indicate that the deformation of the notch tip of concrete mixed with rubber is larger at peak load.

Figure 11 shows the COD distribution of different concrete materials at different loads. It should be noted that in the figure, the negative values indicate the cracking of the material, while

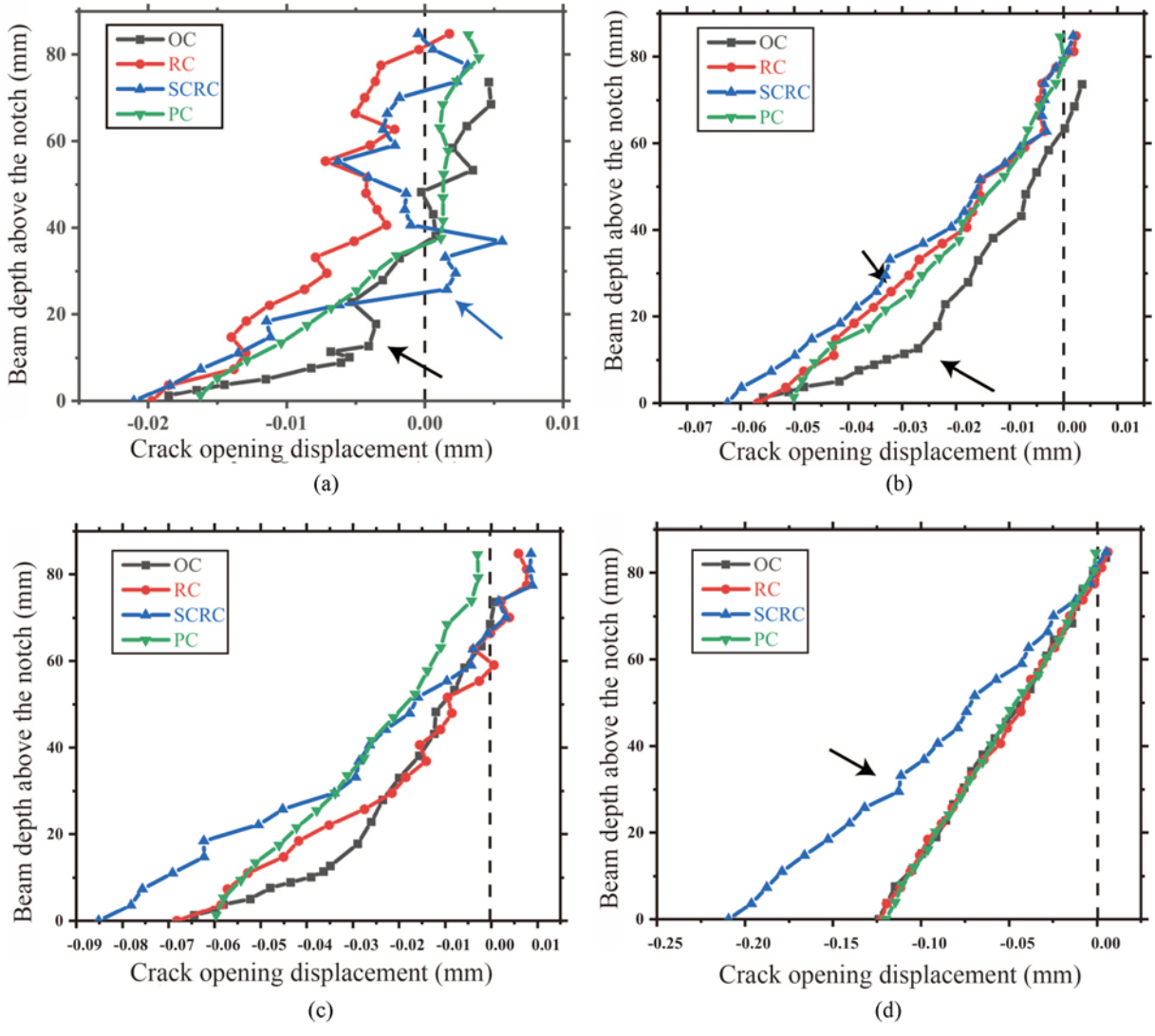

Fig. 11. The COD Distribution along Depth of Different Concrete Materials under Different Loads: (a) 3.5 kN, (b) 2.6 kN in Post-Peak, (c) 2.3 kN in Post-Peak, (d) 1.1 kN in Post-Peak

the positive numbers indicate that the distance between two points decreases, i.e., the compression of the material. It can be seen from the Fig. 11(a) that some areas of the beams show strong resistance to crack. The COD of SCRC fluctuates greatly at the depth of 30 mm, and the COD of OC decreases rapidly with the increase of depth within 10 mm above the notch tip. However, this resistance may gradually vanish during the loading process. From Fig. 11(b), it can be seen that the fluctuation of COD distribution of self-compacting rubber concrete decreases, which indicates the tortuosity for crack propagation may have decreased, and this may be due to the decreased aggregate interlock effect with the crack opening (Guinea et al., 2002; Ritchie, 2011). Toughness is defined as the ability of a material to resist fracture, which depends not only on the bearing capacity of the material, but also on the deformation capacity (Ritchie, 2011). The distributions of COD can reflect the deformations of different materials under a determined load during the fracture process, so it can also show the characteristics of the toughness of the material. It was observed from the Figs. 11(b) – 11(c) that under the same load decrease, the bottom of the CODs of the self-compacting rubber concrete increase more than the other materials, while the upper part of COD curve is close to those of the other specimens. This shows that self-compacting rubber concrete presents better deformation ability, which could promote the dissipation of local high stress that would otherwise result in the fracture of the material. The toughening behavior may be caused by the frictional interlocking of aggregates during fracture, and the presence of rubber particle spanning micro-cracks in concrete (Ritchie, 2011). In post-peak stage, rubber concrete gradually shows the similar deformation capacity as shown in Fig. 11(c). For pervious concrete, the large crack width along the whole beam height and the linear relationship between the COD and the depth is interesting, but not surprising. This can be explained by the fact that the removal of the fine aggregate cause the lack of the bonding force in FPZ to resist cracking in pervious concrete, so the CODs of the upper and bottom part are both large, and the crack opens directly, resulting in the linear relationship between the COD and the depth. In Fig. 11(d), the slope change of COD distribution of concrete materials almost disappears, and the COD distribution of concrete materials is very close except self-compacted rubber concrete. It was observed that the properties of rubber phase in self-compacting rubber concrete is fully developed and make the beam acquire better ductility.

4. Experimental Evaluation of FPZ Development

4.1 FPZ Development of Original Concrete

The fracture process of concrete beams can be studied by combining the P-CMOD curve with the development process of FPZ. The curve of the FPZ-CMOD of original concrete is shown in Fig. 12(a). The contour that corresponds to emerge of the FPZ and the location of the top of FPZ is shown in Fig. 12(b). From the curve of original concrete, it can be seen that the FPZ appears when the load value reaches around 82% peak load, i.e., 2.9 kN. At the initial stage, the FPZ develops slowly, and then it increases drastically with the CMOD value. This behavior may due to the aggregate interlocking, which indicates that the aggregates in FPZ bears high stress in the initial stage (Guinea et al., 2002). At around the 90% maximum load in post-peak field, the FPZ increases greatly, while the slope of load displacement curve decreases correspondingly. This phenomenon indicates that the rapid softening of the cross section with propagation of the FPZ may result in the abrupt decrease in bearing capacity of the specimen.

4.2 FPZ Development of Rubber Concrete

The FPZ-CMOD curve and the image corresponding to the emergence of FPZ of rubber concrete is shown in Fig. 13. It can be seen from the curve that the FPZ emerges when the load value reaches around 2 kN, i.e., 60% of peak load, and this loading stage is earlier than that of original concrete. The length of FPZ increased rapidly in the early stage, and the growth rate slowed down after reaching the peak value. The FPZ propagates at a

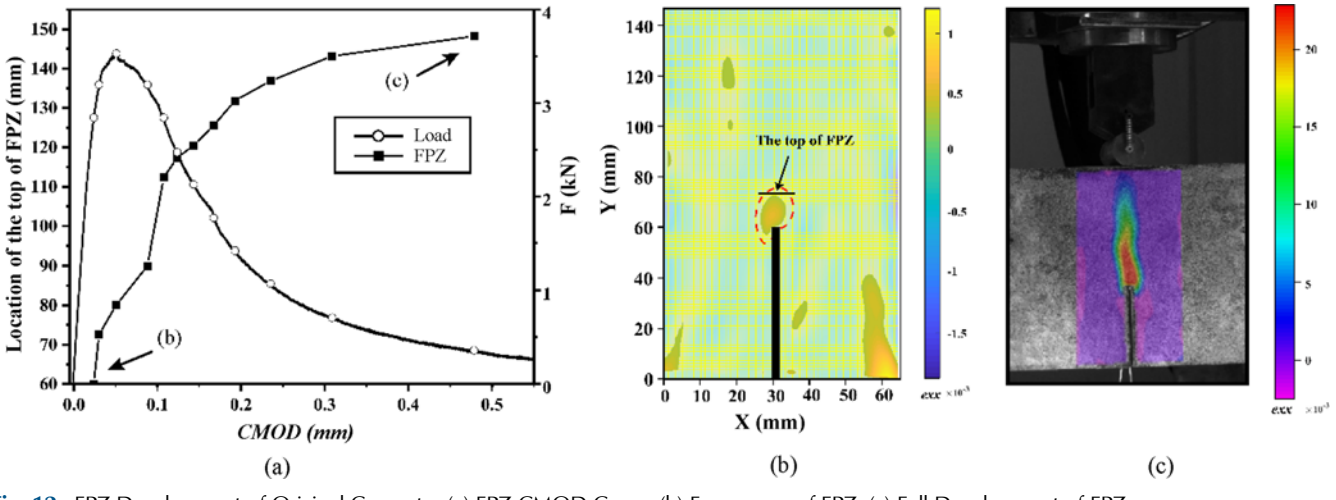

Fig. 12. FPZ Development of Original Concrete: (a) FPZ-CMOD Curve, (b) Emergence of FPZ, (c) Full Development of FPZ

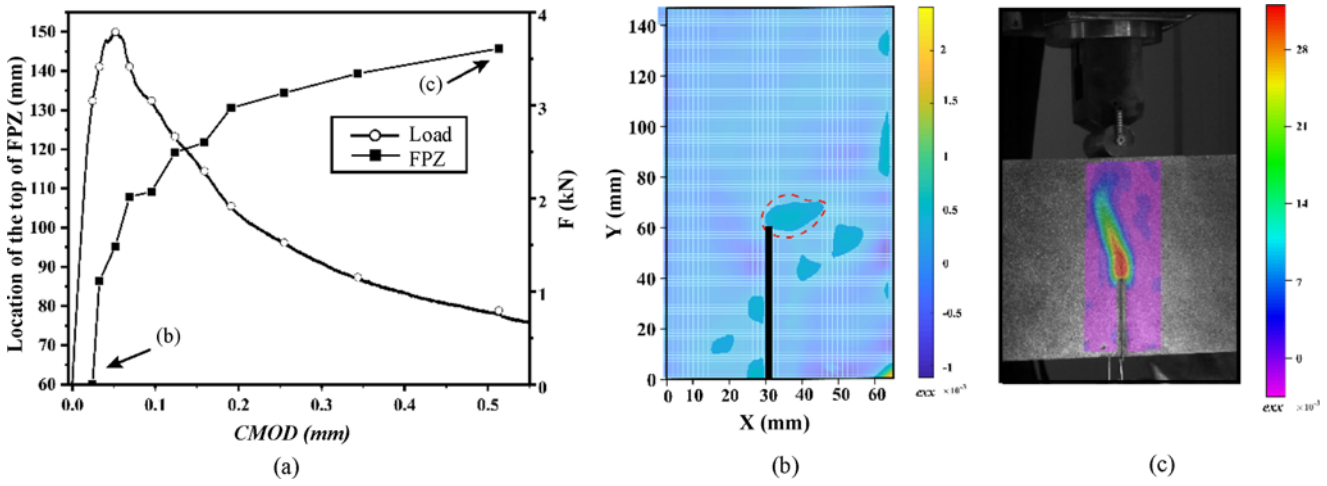

Fig. 13. FPZ Development of Rubber Concrete: (a) FPZ-CMOD Curve, (b) Emergence of FPZ, (c) Full Development of FPZ

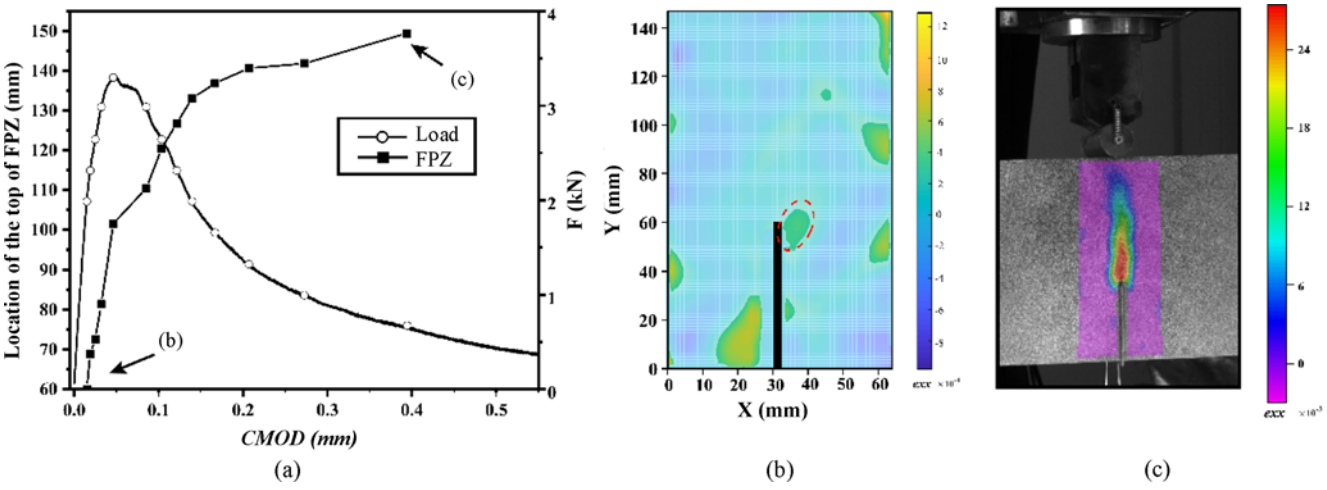

Fig. 14. FPZ Development of Self-Compacting Rubber Concrete: (a) FPZ-CMOD Curve, (b) Emergence of FPZ, (c) Full Development of FPZ

lower rate while the load decreased from maximum load to 90% of the peak. After that, the slope of FPZ growth curve increases, and FPZ turn back to the quick propagation stage.

From the above research, it is found that the FPZ of rubber concrete emerges earlier and develops faster than that of original concrete. The earlier occurrence of FPZ can be attributed to the main reasons as follows: First, the different deformability between rubber and its surrounding cement matrix (Lee et al., 1998), which results in crack initiation around the rubber particles in a fashion similar with that take place with air voids in original concrete (Khatib and Bayomy, 1999). Second, acting as soft aggregate particles under the load, tire rubber particles generate tensile stress on the surface of particles and near the cement paste. This tensile stress leads to premature cracking of cement matrix (Reda Taha et al., 2008); Lastly, the fragile bond between the cement matrix and the rubber particles (Lee et al., 1998). The rubber particles debond from cement matrix causing voids where higher stress concentration generated, so the strength and stiffness decrease is strictly related to the presence of the rubber phase (Li et al., 2004). However, in the post-peak stage, the unique deformation ability of rubber particles can improve the local deformation ability and transfer the tension stress.

4.3 FPZ Development of Self-Compacting Rubberized Concrete

The FPZ-CMOD curve and the emergence of FPZ of self-compacting rubber concrete are shown in Fig. 14. When the FPZ comes out, the load value is between 80% and 90% peak load, which is around 3 kN and close to that of the original concrete.

The load on the self-compacting rubber concrete specimen is larger when the FPZ emerges compared to the rubber concrete. From the length of the FPZ at the peak, it can be observed that the FPZ of self-compacting concrete rubber developed faster than that of ordinary concrete, which may be caused by the addition of rubber. However, even though the rubber content of self-compacting rubber concrete is more than that of rubber concrete, the FPZ length at peak load is shorter than rubber concrete. This may attribute to the self-compacting technology such as the presence of silica fume, which is favorable for binding rubber phases, therefore the porosity is only poorly affected by

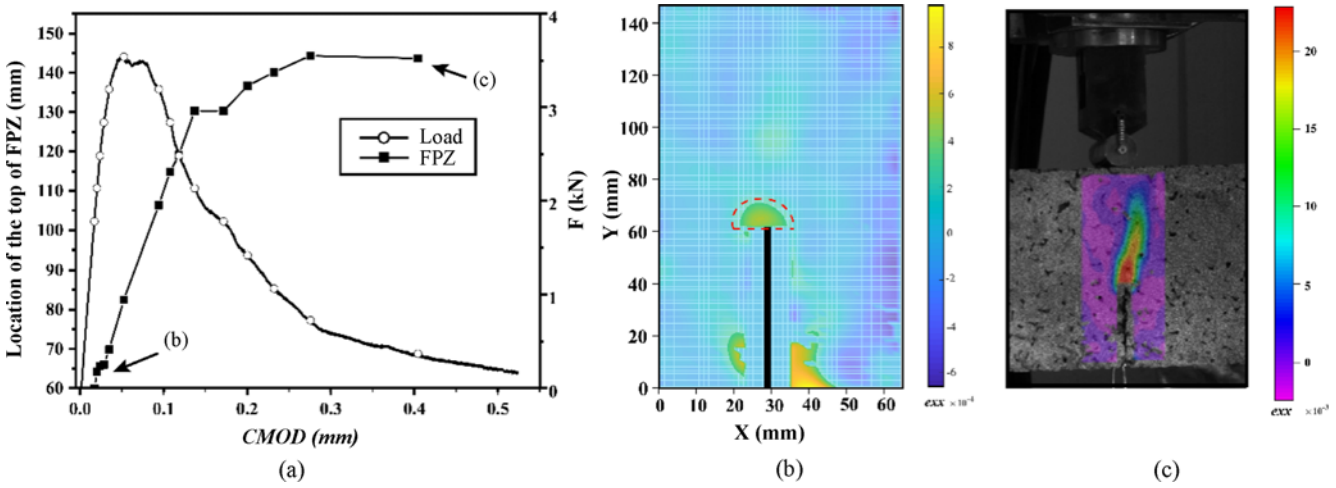

Fig. 15. FPZ Development of Pervious Concrete: (a) FPZ-CMOD Curve, (b) Emergence of FPZ, (c) Full Development of FPZ

the presence of significant amount of rubber phase in comparison with that of ordinary self-compacting concrete (Bignozzi and Sandrolini, 2006). When the peak load is reached, the development of FPZ slows down with the increase of CMOD. It can be seen from the curve that there will be a sudden drop in the load curve when the slope of each FPZ development curve is increased, which indicates that there is a strong correlation between the development of the FPZ and the reduction of post-peak bearing capacity. There are more deceleration behaviors in the propagation of FPZ. Correspondingly, self-compacting rubber concrete has larger fracture energy than other concrete materials. This may be due to the higher content of rubber in self-compacting rubber concrete and the addition of silica fume and superplasticizer, of which the addition is conducive to the porosity reduction in the interface of the cement and rubber. The presence of silica fume in the rubber/cement interface contributes to the better adherence and the recovery of the concrete strength (Pelisser et al., 2011). This characteristic indicates that this concrete material combines the characteristics of low porosity of self-compacting concrete with the toughness behavior of the rubber phase (Bignozzi and Sandrolini, 2006).

4.4 FPZ Development of Pervious Concrete

The FPZ-CMOD curve and the emergence of FPZ of the pervious concrete are shown in the Fig. 15. When the FPZ emerges, the load value is between 50% – 60% of peak load, which is around 2 kN, and it is earlier than that of original concrete. This is mainly caused by the large pores in the pervious concrete, which results in higher strain concentration within the material. The FPZ grows fast after it come out. The length of FPZ increases almost linearly with the increase of CMOD value, and the growth rate remains almost constant until FPZ reaches to 78% of the initial ligament. This shows that the crack in the pervious concrete is easier to develop compared to the original concrete, which may be explained by the fact that due to the lack of interlock and friction between mortar and aggregate, the crack tip is deficient in binding force. This is consistent with the results of COD distribution as shown in Fig. 11.

5. Conclusions

In this paper, the DIC method had been used to calculate the strain and displacement fields on the surface of specimens. DIC technique for measuring the COD and FPZ in concrete beams were reported and discussed. Additionally, the fracture behavior of four different concrete materials has been analyzed. The following conclusions can be drawn:

1. Through the distribution of COD along the height of the specimen, the effect of cohesion in FPZ during the crack development was observed, and with the crack extension and the subsequent pulling out of aggregates, these resistance force to cracking in FPZ gradually failed. Under the same load, the deformation of SCRC is found to be the largest. It also has the largest fracture parameters (K_{IC}^{S} and G_F), which indicates its higher resistance of the material to crack propagation. RC also shows similar properties, but this phenomenon is less obvious, which may be due to its different composition and the rubber particle content. PC had the smallest fracture energy, and the COD distribution shows less cracking-resistance behavior.
2. It is observed that the FPZ emerged before the peak load, and there is a strong correlation between the FPZ and the post-peak strength reduction of concrete. The FPZ growth rate shortly decreased after the peak load and then suddenly rose, corresponding to the nonlinear development of the force value at the peak and the rapid decline of the force in post-peak field. For RC and PC, the FPZ formed at lower loads compared to the OC, which may be related to the change of pore structure and more weak joints in FPZ. It is observed that the rubber particles can improve the local deformation ability in the post-peak field. Additionally, there were more growth rate declining sections in the FPZ development of SCRC, which is consistent with its better toughness.

3. DIC technique was found to be powerful in the quantitative study of FPZ and crack width in concrete. The data of local deformation can be obtained, which can be used to study the crack initiation and propagation process. It showed that this method can be further developed to study the fracture characteristics of other concrete materials. Further research is required to used DIC for studying the relationship between the development of FPZ and the bearing capacity of damaged specimens.

Acknowledgements

This research work was funded by the National Natural Science Foundation of China (No. 51779085), and the Young Elite Scientists Sponsorship Program by China Association for Science and Technology (No. 2017QNRC001) granted to the corresponding author Xudong Chen.

ORCID

Xudong Chen http://orcid.org/0000-0003-0534-6927

References

Arslan ME (2016) Effects of basalt and glass chopped fibers addition on fracture energy and mechanical properties of ordinary concrete: CMOD measurement. *Construction and Building Materials* 114: 383-391, DOI: 10.1016/j.conbuildmat.2016.03.176

Bignozzi MC, Sandrolini F (2006) Tyre rubber waste recycling in self-compacting concrete. *Cement and Concrete Research* 36(4):735-739, DOI: 10.1016/j.cemconres.2005.12.011

Carpinteri A, Fortese G, Ronchei C, Scorza D, Vantadori S (2017) Mode I fracture toughness of fibre reinforced concrete. *Theoretical and Applied Fracture Mechanics* 91:66-75, DOI: 10.1016/j.tafmec.2017.03.015

Dong W, Rong H, Wu Q, Li J (2018) Investigations on the FPZ evolution of concrete after sustained loading by means of the DIC technique. *Construction and Building Materials* 188:49-57, DOI: 10.1016/j.conbuildmat.2018.08.077

Dong W, Zhou X, Wu Z (2013) On fracture process zone and crack extension resistance of concrete based on initial fracture toughness. *Construction and Building Materials* 49:352-363, DOI: 10.1016/j.conbuildmat.2013.08.041

Gali S, Subramaniam KV (2017) Evaluation of crack propagation and post-cracking hinge-type behavior in the flexural response of steel fiber reinforced concrete. *International Journal of Concrete Structures and Materials* 11(2):365-375, DOI: 10.1007/s40069-017-0197-4

Galouei M, Fakhimi A (2015) Size effect, material ductility and shape of fracture process zone in quasi-brittle materials. *Computers and Geotechnics* 65:126-135, DOI: 10.1016/j.compgeo.2014.12.010

Ghamgosar M, Erarslan N (2016) Experimental and numerical studies on development of fracture process zone (FPZ) in rocks under cyclic and static loadings. *Rock Mechanics and Rock Engineering* 49(3): 893-908, DOI: 10.1007/s00603-015-0793-z

Guan D, Guo Z, Jiang C, Yang S, Yang H (2019) Experimental evaluation of precast concrete beam-column connections with high-strength steel rebars. *KSCE Journal of Civil Engineering* 23(1):238-250, DOI: 10.1007/s12205-018-1807-7

Guinea GV, El-Sayed K, Rocco CG, Elices M, Planas J (2002) The effect of the bond between the matrix and the aggregates on the cracking mechanism and fracture parameters of concrete. *Cement and Concrete Research* 32(12):1961-1970, DOI: 10.1016/S0008-8846(02)00902-X

Guo Y, Chen X, Li X, Li S, Guo S (2019) Experimental study on fracture behavior of three-graded concrete under cyclic loading after initial static loading. *Theoretical and Applied Fracture Mechanics* 103:102272, DOI: 10.1016/j.tafmec.2019.102272

Hu XZ, Wittmann FH (1992) Fracture energy and fracture process zone. *Materials and Structures* 25(6):319-326, DOI: 10.1007/BF02472590

Ibrahim A, Mahmoud E, Yamin M, Patibandla VC (2014) Experimental study on Portland cement pervious concrete mechanical and hydrological properties. *Construction and Building Materials* 50: 524-529, DOI: 10.1016/j.conbuildmat.2013.09.022

Jenq Y, Shah SP (1985) Two parameter fracture model for concrete. *Journal of Engineering Mechanics* 111(10):1227-1241, DOI: 10.1061/(ASCE)0733-9399(1985)111:10(1227)

Khatib ZK, Bayomy FM (1999) Rubberized Portland cement concrete. *Journal of Materials in Civil Engineering* 11(3):206-213, DOI: 10.1061/(ASCE)0899-1561(1999)11:3(206)

Kim KW, El Hussein M (1997) Variation of fracture toughness of asphalt concrete under low temperatures. *Construction and Building Materials* 11(7-8):403-411, DOI: 10.1016/S0950-0618(97)00030-5

Kim SW, Lee SS, Kim NS, Kim DJ (2013) Numerical model validation for a prestressed concrete girder bridge by using image signals. *KSCE Journal of Civil Engineering* 17(4):509-517, DOI: 10.1007/s12205-013-0560-1

Kozicki J, Tejchman J (2007) Experimental investigations of strain localization in concrete using digital image correlation (DIC) technique. *Archives of Hydro-Engineering and Environmental Mechanics* 54(1):3-24

Lee HS, Lee H, Moon JS, Jung HW (1998) Development of tire added latex concrete. *Materials Journal* 95(4):356-364

Li G, Stubblefield MA, Garrick G, Eggers J, Abadie C, Huang B (2004) Development of waste tire modified concrete. *Cement and Concrete Research* 34(12):2283-2289, DOI: 10.1016/j.cemconres.2004.04.013

Marar K, Eren Ö Roughani H (2017) The influence of amount and aspect ratio of fibers on shear behaviour of steel fiber reinforced concrete. *KSCE Journal of Civil Engineering* 21(5):1393-1399, DOI: 10.1007/s12205-016-0787-2

Meng W, Yao Y, Mobasher B, Khayat KH (2017) Effects of loading rate and notch-to-depth ratio of notched beams on flexural performance of ultra-high-performance concrete. *Cement and Concrete Composites* 83:349-359, DOI: 10.1016/j.cemconcomp.2017.07.026

Mirzazadeh MM, Green MF (2018) Fiber optic sensors and digital image correlation for measuring deformations in reinforced concrete beams. *Journal of Bridge Engineering* 23(3), DOI: 10.1061/(ASCE)BE.1943-5592.0001189

Mirzazadeh MM, Noël M, Green MF (2016) Effects of low temperature on the static behaviour of reinforced concrete beams with temperature differentials. *Construction and Building Materials* 112:191-201, DOI: 10.1016/j.conbuildmat.2016.02.216

Otsuka K, Date H (2000) Fracture process zone in concrete tension specimen. *Engineering Fracture Mechanics* 65(2-3):111-131, DOI: 10.1016/S0013-7944(99)00111-3

Pelisser F, Zavarise N, Longo TA, Bernardin AM (2011) Concrete made with recycled tire rubber: Effect of alkaline activation and silica fume addition. *Journal of Cleaner Production* 19(6-7):757-763,

DOI: 10.1016/j.jclepro.2010.11.014

Rechenmacher AL, Finno RJ (2004) Digital image correlation to evaluate shear banding in dilative sands. *Geotechnical Testing Journal* 27(1):13-22, DOI: 10.1520/GTJ11263J

Reda Taha MM, El-Dieb AS, Abd El-Wahab MA, Abdel-Hameed ME (2008) Mechanical fracture and microstructural investigations of rubber concrete. *Journal of Materials in Civil Engineering* 20(10): 640-649, DOI: 10.1061/(ASCE)0899-1561(2008)20:10(640)

Ritchie RO (2011) The conflicts between strength and toughness. *Nature Materials* 10(11):817-822, DOI: 10.1038/nmat3115

Rossi M, Lava P, Pierron F, Debruyne D, Sasso M (2015) Effect of DIC spatial resolution noise and interpolation error on identification results with the VFM. *Strain* 51(3):206-222, DOI: 10.1111/str.12134

Saouma VE, Broz JJ, Brühwiler E, Boggs HL (1991) Effect of aggregate and specimen size on fracture properties of dam concrete. *Journal of Materials in Civil Engineering* 3(3):204-218, DOI: 10.1061/(ASCE)0899-1561(1991)3:3(204)

Sayadi A, Neitzert TR, Clifton GC, Han MC, De Silva K (2018) Ultra-lightweight concrete containing expanded poly-lactic acid as lightweight aggregate. *KSCE Journal of Civil Engineering* 22(10):4083-4094, DOI: 10.1007/s12205-018-1976-4

Shah SP (1990) Determination of fracture parameters (K_{IC}^{S} and $CTOD_c$) of plain concrete using three-point bend tests. *Materials and Structures* 23: 457-460, DOI: 10.1007/BF02472029

Thomas BS, Gupta RC (2015) Long term behaviour of cement concrete containing discarded tire rubber. *Journal of Cleaner Production* 102: 78-87, DOI: 10.1016/j.jclepro.2015.04.072

Wittman FH (1985) Determination of the fracture energy of mortar and concrete by means of three-point bend tests on notched beams. *Materials and Structures* 18(106):285-290, DOI: 10.1007/BF02472918

Wu Z, Rong H, Zheng J, Xu F, Dong W (2011) An experimental investigation on the FPZ properties in concrete using digital image correlation technique. *Engineering Fracture Mechanics* 78(17): 2978-2990, DOI: 10.1016/j.engfracmech.2011.08.016

Xu J, Fu Z, Han Q, Lacidogna G, Carpinteri A (2018) Micro-cracking monitoring and fracture evaluation for crumb rubber concrete based on acoustic emission techniques. *Structural Health Monitoring* 17(4):946-958, DOI: 10.1177/1475921717730538

Xu S, Zhang X (2008) Determination of fracture parameters for crack propagation in concrete using an energy approach. *Engineering Fracture Mechanics* 75(15):4292-4308, DOI: 10.1016/j.engfracmech.2008.04.022

Yang RC (2014) A regularized finite-element digital image correlation for irregular displacement field. *Optics and Lasers in Engineering* 56:67-73, DOI: 10.1016/j.optlaseng.2013.12.013

Yang J, Jiang G (2003) Experimental study on properties of pervious concrete pavement materials. *Cement and Concrete Research* 33(3): 381-386, DOI: 10.1016/S0008-8846(02)00966-3

Yaofeng S, Pang JHL (2007) Study of optimal subset size in digital image correlation of speckle pattern images. *Optics and Lasers in Engineering* 45(9):967-974, DOI: 10.1016/j.optlaseng.2007.01.012

Yuan J, Chen X, Liu S, Li S, Shen N (2018) Effect of water head, gradation of clogging agent, and horizontal flow velocity on the clogging characteristics of pervious concrete. *Journal of Materials in Civil Engineering* 30(9):04018215, DOI: 10.1061/(ASCE)MT.1943-5533.0002410

Yung WH, Yung LC, Hua LH (2013) A study of the durability properties of waste tire rubber applied to self-compacting concrete. *Construction and Building Materials* 41:665-672, DOI: 10.1016/j.conbuildmat.2012.11.019

Zhang Z, Ansari F (2005) Crack tip opening displacement in micro-cracked concrete by an embedded optical fiber sensor. *Engineering Fracture Mechanics* 72(16):2505-2518, DOI: 10.1016/j.engfracmech.2005.03.007

Zhao YR, Wang L, Lei ZK, Han XF, Xing YM (2017) Experimental study on dynamic mechanical properties of the basalt fiber reinforced concrete after the freeze-thaw based on the digital image correlation method. *Construction and Building Materials* 147:194-202, DOI: 10.1016/j.conbuildmat.2017.02.133

Zhu R, Xie H, Hu Z, Jiang L, Guo B, Li C (2015) Performances of different subset shapes and control points in subset-based digital image correlation and their applications in boundary deformation measurement. *Applied Optics* 54(6):1290-1301, DOI: 10.1364/AO.54.001290